

Exotic electronic states in gradient-strained untwisted graphene bilayers

Zeyu Liu^{1,2,3,#}, Xianghua Kong^{1,#*}, Zewen Wu^{1,#}, Linwei Zhou^{1,2,3}, Jingsi Qiao⁴ and Wei Ji^{2,3,*}

¹*College of Physics and Optoelectronic Engineering, Shenzhen University, Shenzhen 518060, China.*

²*Beijing Key Laboratory of Optoelectronic Functional Materials & Micro-nano Devices, Department of Physics, Renmin University of China, Beijing 100872, China*

³*Key Laboratory of Quantum State Construction and Manipulation (Ministry of Education), Renmin University of China, Beijing, 100872, China*

⁴*Advanced Research Institute of Multidisciplinary Sciences & School of Integrated Circuits and Electronics, Beijing Institute of Technology, Beijing 100081, China*

**Correspondence and request for materials should be addressed to: kongxianghuaphysics@szu.edu.cn (X.K.), wji@ruc.edu.cn (W.J.),*

ABSTRACT: Many exotic electronic states were discovered in moiré superlattices hosted in twisted homo-bilayers in the past decade, including unconventional superconductivity and correlated insulating states. However, it is technically challenging to precisely and orderly stack two or more layers into certain twisting angles. Here, we presented a theoretical strategy that introduces moiré superlattices in untwisted homo-bilayers by applying different in-plane strains on the two layers of a graphene homo-bilayer, respectively. Our density functional theory calculations indicate that the graphene bilayer exhibits substantial out-of-plane corrugations that form a coloring-triangular structure in each moiré supercell under gradient in-plane strains. Such structure leads to a set of kagome bands, namely one flat-band and, at least, one Dirac band, developing along the M-K path after band-folding. For comparison, uniformly applied in-plane strain only yields a nearly flat band within path K-G, which is originated from local quantum confinement. These findings highlight the gradient strain as a route to feasibly fabricate exotic electronic states in untwisted flexible homo-bilayers.

Introduction

Periodic moiré patterns can arise from the stacking of two-dimensional (2D) materials, either homogeneous or heterogeneous, using methods such as rotation or lattice mismatch. The wide range of available 2D materials and twist angles provides a broad platform for wavelength and symmetry modulation of moiré patterns¹. When the twist angle between two neighboring layers in twisted moiré patterns is small enough, their atomic structures will undergo reconstruction, resulting in the formation of isolated flat bands in the folded mini-Brillouin zone²⁻⁴. These flat bands are accompanied by enhanced electron-electron interactions near their vicinity, giving rise to phenomena like Wigner crystals, correlated insulators, and unconventional superconductivity^{5,6}. In addition, the slowly varying moiré potential in moiré superlattices significantly promotes the formation of moiré excitons, including moiré inter- and intralayer excitons, as well as moiré trions⁷⁻⁹.

However, even a slight structural perturbation can result in significantly different properties within a moiré pattern. For example, in the magic-angle graphene system, the superconducting states may disappear under an angular and moiré wavelength fluctuation of only 0.1° and 1 nm, respectively^{10,11}. Therefore, establishing a link between the twist angle and the electronic properties of moiré pattern is challenging. Furthermore, when introducing twist, most current experimental assembly techniques inevitably lead to unpredictable strain fluctuations, known as moiré disorder¹²⁻¹⁵. This moiré disorder greatly hinders the reproducibility of experiments and the alignment with theoretical findings¹⁶⁻²⁰. Thus, the precision of twist angles and the presence of moiré disorder in experimental research pose formidable obstacles to the deeper exploration of moiré superlattices. Consequently, a few moiré superlattices were constructed in untwisted bi- or few-layers. Fractional Chern insulating states were discovered in untwisted but periodically strained monolayer graphene²¹. Lattice mismatched but untwisted bilayers were also used to build moiré lattices in the literature. A two-atom-layer Bi (110) stacking on the SnSe (001) substrate forms a moiré superlattice that exhibits one-dimensional flat bands without layer twisting²².

Furthermore, untwisted 2D metal-organic nanosheets were shown to be more effective in high-resolution separation of para-/meta-isomers pairs compared to their twisted counterparts²³.

Ever since the successful exfoliation of graphene, its remarkable electrical, optical, and mechanical properties have been the subject of extensive investigations and practical applications. Notably, graphene is the strongest 2D material ever measured, with an intrinsic strength of 130 GPa and a Young's modulus of 1 TPa. It can endure a reversible tensile strain up to 25%²⁴⁻²⁷. Therefore, graphene is an idea platform of producing moiré patterns based on the easy implementation of strain. Previous reports have shown that by applying a bubble structure, bilayer graphene exhibits a strain difference of about 2% between the two layers²⁸⁻³². Based these facts, we present a theoretical study on the bilayer graphene moiré pattern induced by biaxial strain rather than twist angle. This strain-induced moiré pattern can be easily realized in the laboratory, as it avoids the need for high-precision twist angles. Moreover, the strain-induced moiré pattern creates out-of-plane undulations and generates a new moiré potential field after relaxation. We refer to this as gradient-strain bilayer graphene (GSBG).

Various effective theoretical models were used to model or predict physical properties of graphene moiré superlattices, which have shown relatively good agreement with experiments³³⁻³⁷. However, by scaling system size down, this approach neglects certain microscopic effects, such as non-homogeneous variations of strain and the transitions between high symmetry stacking regions. Furthermore, it heavily relies on a variety of empirical parameters. In this study, we employed first-principles calculations to investigate the electronic properties of bilayer graphene moiré patterns before and after geometry optimization. The results, with significantly higher precision, provide us deeper insights into microscopic mechanisms underlying flat bands. These bands originate from the synergy of the interlayer coupling effect, which is modulated by the periodic moiré potential and gradient-strain. It is also demonstrated that gradient-strain can act as a new method for constructing moiré patterns with unique emerging electronic states.

Models

To create a moiré lattice in bilayer graphene using strain, we utilized two graphene monolayers with supercells of $3N-1 \times 3N-1$ and $3N \times 3N$, respectively. Biaxial tensile and compressive strains were applied to the respective monolayers, ensuring a zero-lattice mismatch. The resulting moiré superlattice is referred to 'average strain bilayer graphene', as shown in Fig. 1(a). This moiré pattern exhibits four distinct high-symmetry stacking configurations: AA, AB, BA and SP stacking, as illustrated in the right half of Fig. 1(b). In AA stacking, the upper carbon atoms align perfectly with their counterparts in the lower layer. AB and BA stacking correspond to the alignment of the two sublattices of the upper graphene layer with the hollow sites of the lower graphene layer, respectively. Additionally, there exists a transitional stacking structure known as SP stacking. It is important to note that the lower graphene layer was selected as a $3N \times 3N$ supercell, facilitating analysis using band folding technique. Specifically, we observed that the Dirac cone of the upper graphene layer remained located at the K-point within the folded Brillouin zone, while the Dirac cone of the lower graphene layer transitioned from the K-point to the Γ -point, as shown in Fig. 1(f)³⁸.

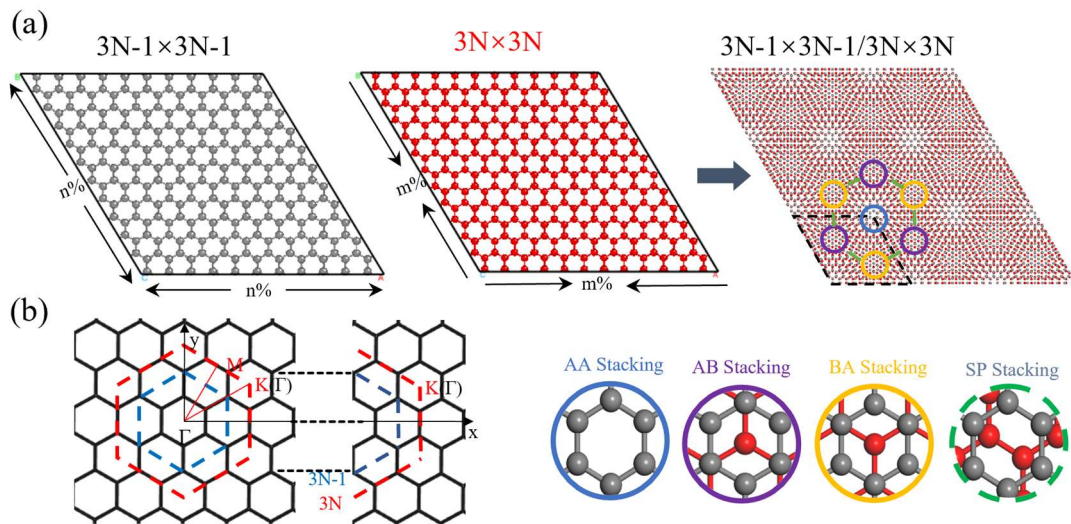


Figure 1 (a) Schematic diagram of average strain bilayer graphene construction consisting of the upper (gray) and lower (red) layers of graphene subjected to tensile or compressive strains bonded together by van der Waals forces, and the black dashed lines indicate the calculated superlattices. As shown in the

lower right corner, different colors indicate different high symmetry stackings in Fig. (a). (b) Schematic representation of the Brillouin zone and its folding.

Methods

Density functional theory calculations were performed using the generalized gradient approximation (GGA) with the Perdew-Burke-Ernzerhof (PBE) for the exchange-correlation potential, linear combined atomic orbitals (LCAO) method, and a single-zeta polarized (SZP) atomic orbital basis set as implemented in the RESCU package³⁹. The real space mesh resolution was set to 0.35 Bohr, and the convergence criteria for electronic energy and charge density are both set to 10^{-5} to ensure good convergence. Two k -meshes of $3 \times 3 \times 1$ and $1 \times 1 \times 1$ were adopted for calculations on the $11 \times 11 + 12 \times 12$ and $35 \times 35 + 36 \times 36$ supercells, respectively. The lattice constant of the graphene primitive cell is 2.4612 Å. The system has a vacuum thickness up to about 56 Å in the z -direction to avoid interactions due to periodicity at the surface. All structural relaxations of the homogeneously strain graphene bilayers were performed using the implementation of a force field, facilitated by the Large Atomic/Molecular Massively Parallel Simulator (LAMMPS)⁴⁰. The C-C interactions within each graphene layer were described using a many-body Tersoff potential, while the interlayer van der Waals interactions were accounted via the Kolmogorov-Crespi (KC) potential^{41,42}. All atoms were fully relaxed until the residual force per atoms was less than 1.0×10^{-4} eV/Å.

Results and Discussion

Flat-sheet bilayer graphene under uniform in-plane strain

By adjusting the system size, denoted by N , a series of moiré superlattices can be constructed. Each moiré superlattice possesses its own unique strain rate (Fig. S1(a)). For instance, in a system with a size of $35 \times 35 + 36 \times 36$ ($N=12$), the upper layer experiences a biaxial tension strain with a rate of 1.41%, while the lower layer undergoes a biaxial compression strain with a rate of -1.41%, resulting an average strain rate of 1.41%. In other words, the introduced average strain is determined by the system size. Moreover, the average strain can regulate the moiré potentials in different

periodicity and the intralayer distance between different high-symmetry stackings. In this study, we first investigated the properties of the flat-sheet bilayer graphene constructed by uniform in-plane strain.

In such flat-sheet moiré system, the bandwidth of the Dirac band along K- Γ high symmetry path around the fermi energy is effectively adjusted by the magnitude of strain in the system. As shown in Fig. 2(a, b) and Fig. S1(b), when the interlayer space (d) is fixed at 3.3 Å, the bandwidth of the Dirac states- related band (marked as red line) significantly narrows from 380 to 25 meV, as the system size increases and the strain magnitude decreases from 4.35% to 1.41%. Consequently, the Dirac bands within the pristine upper graphene layer become relatively flat, indicating the modulation of the moiré potential by stain (See Supplementary Material for details). This strain also generates a moiré potential field with a long wavelength, effectively reshaping the corresponding electronic band structure.

The electronic properties of average strained bilayer graphene can also be adjusted by its interlayer space. It is well known that an increased interlayer spacing can significantly weaken or even completely inhibit the interlayer coupling of 2D materials, leading to modified electronic properties^{36,37}. By keeping the stain rate constant, we investigated the modulation effect of interlayer spacing on average strained bilayer graphene by adjusting it from 3.3 Å to 3.5 Å. As exhibited in Fig. 2(b) and 2(c), the Dirac state along K- Γ effectively restores its monolayer characteristics, with its bandwidth increasing to 128 meV.

The emergence flat bands along the K- Γ path originates from the redistribution of charge density in real space. For simplicity, we label the original Dirac states as O_a , O_b and O_c (represented by the red line in Fig. 2), and their corresponding real space charge density as $|\psi_{O_a}|^2$, $|\psi_{O_b}|^2$ and $|\psi_{O_c}|^2$, respectively (shown in Fig. 2(d-f)). Firstly, when comparing $|\psi_{O_a}(r)|^2$ (with an average strain rate of 4.35%) to $|\psi_{O_b}(r)|^2$ (with an average strain of 1.41%), the later experiences a specific periodic moiré potential and exhibits a significantly different distribution. The charge density is localized on the upper layer in AB/BA stacking regions and on the lower layer in AA stacking regions,

as shown in Fig. 2(e). As a result, the Dirac electronic state of the upper graphene layer along the K- Γ is strongly modulated, leading to a nearly-flat band. It's evident from our study (Fig. 2 and Supplementary Figures) that a smaller average strain rate results in a flatter Dirac band, which warrants further exploration. Secondly, under the same strain, as the interlayer spacing increases, the real space distribution of charge density in the Dirac band reverts back to the case of a large strain rate, as shown in Fig. 2(f). Due to the weakened interlayer coupling, the charge initially localized on the upper layer in AB/BA stacking regions dissipates in the charge density $|\psi_{O_c}(r)|^2$ compared to $|\psi_{O_b}(r)|^2$. Consequently, the Dirac band returns to its linear-cone characteristic. Conversely, the charge initially localized on the lower graphene layer in AA regions maintains its localization, owing to the persistent effects of periodic moiré potential and interlayer interaction. Furthermore, by comparing $|\psi_{O_c}(r)|^2$ and $|\psi_{O_a}(r)|^2$, it can be revealed that this phenomenon likely originates from the Dirac state contributed by the lower graphene layer.

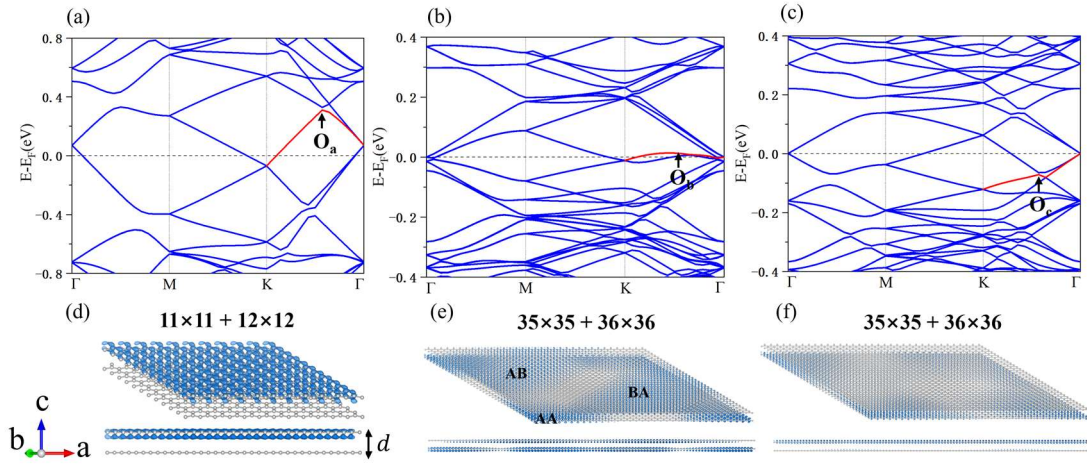


Figure 2. Electronic properties of average strain bilayer graphene. (a-c) band structures. (a) an average strain of 4.35%; (b, c) an average strain of 1.41%. (a, b) an interlayer space of 3.3 Å; (c) an interlayer space of 3.5 Å. (d-e) real space distributed charge densities corresponding to the states marked with O_a , O_b and O_c , respectively. The isosurface of (d) and (e-f) is $1.8 \times 10^{-4} e \text{ \AA}^{-3}$ and $3.7 \times 10^{-5} e \text{ \AA}^{-3}$, respectively.

“Three-dimensional” bilayer graphene under gradient in-plane strains

Based on the previous structures of average strained flat-sheet bilayer graphene, a

new structure called gradient-strain bilayer graphene (GSBG) was obtained through fully Molecular Dynamics (MD) relaxation. Interestingly, the final relaxed atomic structure remains the same, regardless of the changes in the initial average strain rate and interlayer spacing. After releasing the out-of-plane confinement, the atomic structure displays undulations and gradient strain, which can be characterized by a concave 'Mercedes-Benz label' centered at AA stacking region, surrounded by peak-like AB/BA stacking regions, as shown in Fig. 3(a, b). This structure exhibits a triple rotational symmetry. On one hand, in the out-of-plane direction, the GSBG structure achieves its lowest formation energy by increasing the interlayer spacing in AA stacking regions and maintaining the lowest interlayer spacing globally in AB/BA stacking regions, consistent with experimental observations⁴³. On the other hand, in the atomic plane, GSBG maximizes the area of the most favorable stacking configurations and releases the lattice elastic energy primarily by adjusting the out-of-plane strain in the transition regions.

Furthermore, when treating different stacking configurations as distinct “superatoms”, the GSBG resembles a squeezed Coloring Triangle (CT) lattice⁴⁴, as illustrated by the highlighted lines in Fig. 3(a). This insight into the atomic geometry inspires a new way to characterize the electronic structure of GSBG, as shown in Fig. 3(c). Specifically, a flat band with a band width of approximately 8.1 meV is observed on a segment of the highly symmetric path in the first Brillouin zone. This flat band is accompanied by two bands forming a Dirac cone above it, which degenerate with it at each end, as highlighted by the red lines in Fig. 3(c). Clearly, these elements constitute the typical three energy bands of a CT lattice⁴⁵. These phenomena are robust regardless of the size of GSBG. The CT lattice and its characteristic three-bands, especially the flat band, are prevalent in GSBG systems with smaller sizes, as shown in Fig. S4. Therefore, it can be concluded that the emergence of an adjustable flat band along the M-K path is attributed to the appearance of long-wavelength moiré potential after the reconfiguration of the atomic structure.

Further analysis of the real space distributed charge density in the GSBG system has revealed additional features of CT lattice. In Fig. 3(d), the charge density

distribution of the state on the flat band (highlighted by the red line in Fig. 3(c)) at the K point is presented. Firstly, as a consequence of the triple rotational symmetry in GSBG, the charge vanishes in the AA stacking region due to the destructive interference of quantum geometric effects. Secondly, the charge demonstrates an expansion at the CT-like lattice point, indicating the presence of charge accumulation in these regions. Thirdly, the charge is distributed on both graphene layers, as shown in Fig. S5. This observation suggests a relatively strong interlayer coupling between the layers.

The interlayer coupling, which indicates the emergence of flat band, can also be revealed through the interlayer charge transfer in GSBG. As shown in the charge density distribution (DCD) in Fig. 3(e), there is a charge transfer of 3.27×10^{-4} e/atom from the lower to the upper graphene layer in the GSBG. Specifically, there is minimal charge transfer in AA stacking regions due to the large interlayer spacing. In contrast, significant charge transfer occurs in the transition stacking regions, while there is little charge transfer in the AB/BA regions due to the large misalignment of atoms between the two layers (Fig. S5). Importantly, the monotonic variation of DCD with interlayer spacing highlights the direct relationship between interlayer charge transfer and interlayer spacing. Furthermore, the one-way interlayer charge transfer in GSBG also leads to an out-of-plane polarization. As shown in Fig. 4(f), the polarization in GSBG predominantly occurs in the non-highly symmetric stacking region. This polarization is induced by the inhomogeneous charge distribution between the upper and lower layers, which results in the structural reconfiguration.

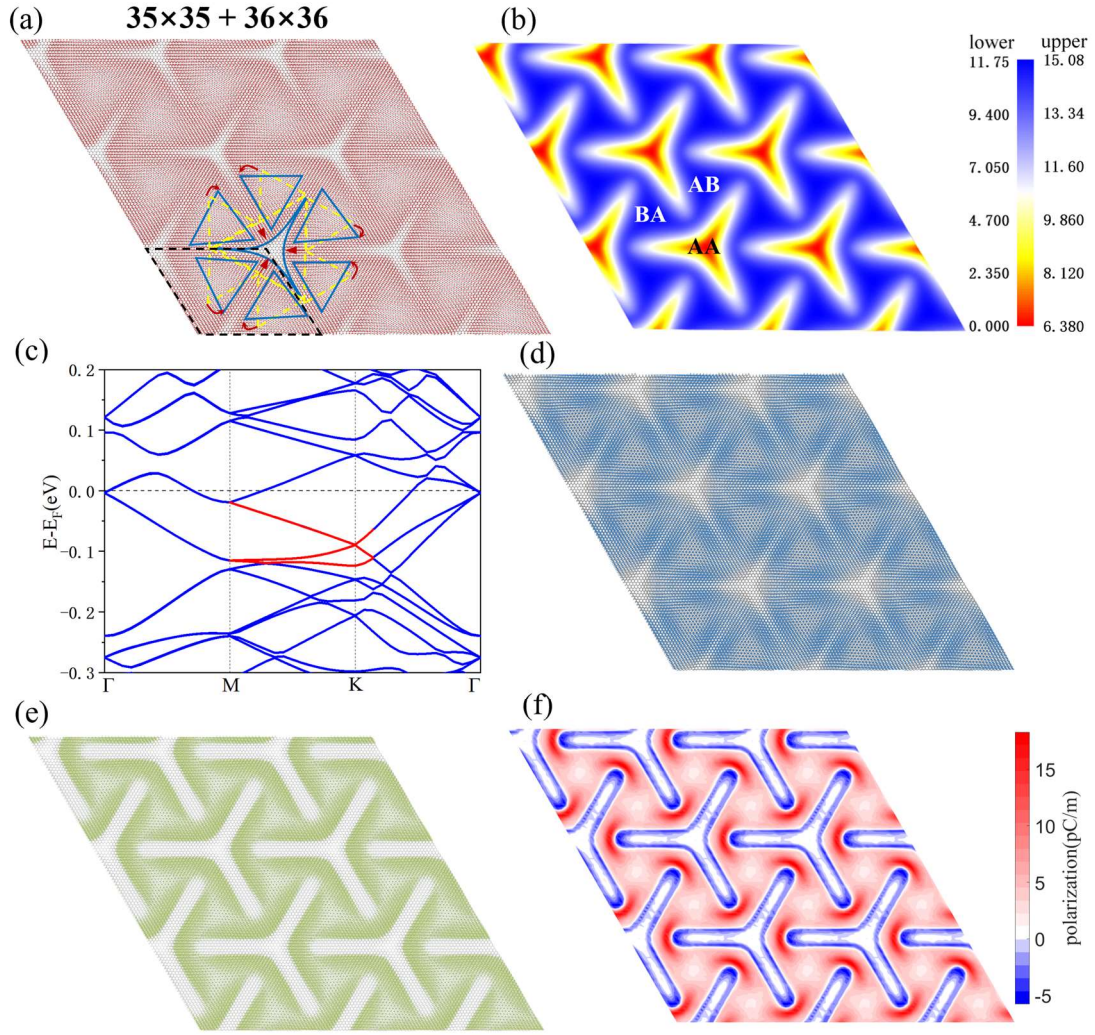


Figure 3. Atomic structure and electronic properties of gradient-strain bilayer graphene. (a) Top view of the atomic structure, which has an average strain of 1.41%. The dashed black line, dashed yellow line and solid blue line indicates a supercell, the Colored Triangular (CT) lattice and the evolved structural features, respectively. (b) Out-of-plane fold amplitude of the upper and lower graphene layers, unit in Å. (c) The energy band structure of the relaxed structure. (d) Real-space distribution of mode-squared wave function $|\psi_n(r)|^2$ of the red flat bands at K point in (c). (e) Differential Charge Density distribution (DCD) $\Delta\rho = \rho_{bilayer} - \rho_{upper} - \rho_{lower}$, with yellow representing positive and blue representing negative. The isosurface values of the wavefunction and the DCD are $1 \times 10^{-5} \text{ e \AA}^{-3}$ and $5 \times 10^{-5} \text{ e \AA}^{-3}$. (f) The distribution of polarization intensity of Gradient-Strain Bilayer Graphene.

The emergence of new physical properties primarily arises from geometric reconfiguration. Deeper insights into this gradient-strain moiré superlattice are

manifested through the distribution of gradient-strain, which can be characterized by changes in interatomic bond lengths. On one hand, after the release of the out-of-plane strain, atoms in both layers move synchronously in the out-of-plane direction, resulting in a corrugation. Consequently, the upper and lower layers exhibit similar out-of-plane strain profiles, as depicted in Fig. 4(a) and (c). Furthermore, the out-of-plane strain disappears in the AA and AB/BA stacking regions, protected by inversion symmetry, but emerges in the transition stacking regions. This behavior is opposite to the distribution of polarization, suggesting their lack of correlation. Meanwhile, the BA and AB regions exhibit opposite out-of-plane strain, inducing a strain gradient magnitude transitioning from the BA to AB stacking region, as shown by the colored arrow in Fig. 4(a). On the other hand, both the upper and lower graphene layers exhibit clear in-plane gradient-strain characteristics, as shown in Fig. 4(b) and (d). However, due to the initially imposed compressive strain, the lower graphene layer displays the simultaneous presence of both compressive and tensile strains across the in-plane direction. Importantly, the regions of compressive strain (red region in Fig. 4(b)) coincide with the electric polarized regions in Fig. 3(f). This directly indicates the synergistic modulation of out-of-plane and in-plane gradient-strain on the polarization of the system.

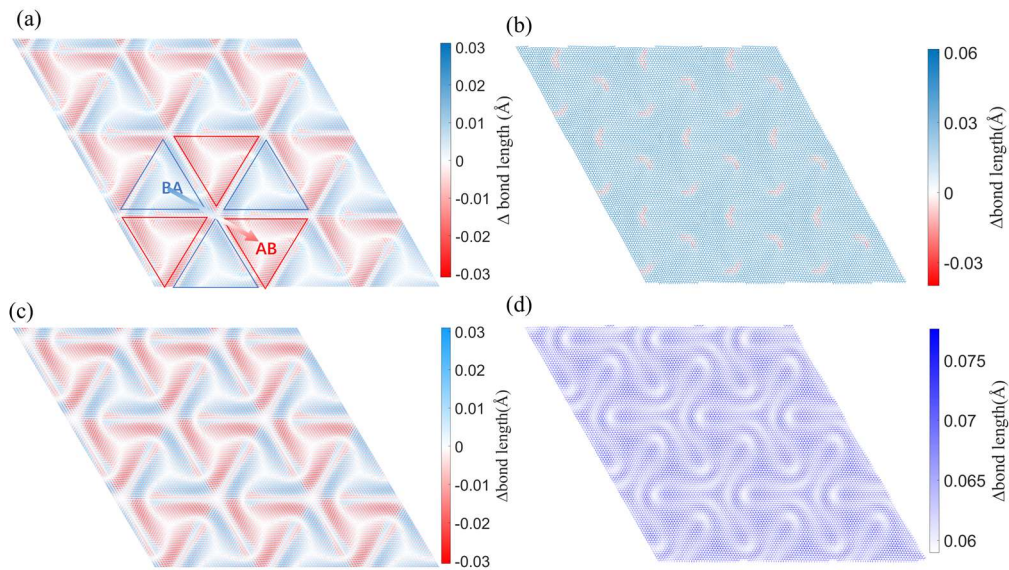


Figure 4 Strain distributions in the lower (a, b) and the upper (c,d) graphene layers graphene layers for the out-of-plane (a, c) and in-plane (b,d) strain distributions.

Conclusion

In this study, we investigated the electronic states of gradient-strain bilayer graphene, considering both average and gradient strain, using first-principles calculations. In structures of average strain, we observed the emergence of flat bands along the K- Γ path in momentum space, which was found to be influenced by both in-plane strain and interlayer spacing. By analyzing the charge density distribution of these states in real-space, we determined that these flat bands are primarily a result of size effects and interlayer coupling. In the case of gradient-strain bilayer graphene, the introduction of out-of-plane gradient-strain leads to the formation of a moiré pattern resembling a CT lattice. This structural transformation gives rise to a tunable flat band along the M-K path, with the corresponding charge being localized in specific regions in real-space. This localization may be attributed to the destructive interference of quantum geometric effects. Additionally, the analysis of electric polarization intensity and gradient-strain distribution, highlights the significance of transition stacking regions in moiré pattern. These findings reveal a novel mechanism that combines moiré potential with gradient strain to generate emergent electronic states. In summary, we have proposed an innovative methodology for constructing moiré patterns and investigating the resulting electronic states. Furthermore, by inducing different gradient strain fields, it is possible to design distinct electronic states. This exploration can be extended to other 2D materials, offering intriguing possibilities and novel insights for the design of energy bands in flexible electronic devices.

Acknowledges: This work was financially supported by the National Key R&D Program of China (Grant No. 2018YFE0202700), the National Natural Science Foundation of China (Grants No. 11974422, No. 12104313, and No. 12204534), the Department of Science and Technology of Guangdong Province (No. 2021QN02L820) and the Shenzhen Natural Science Fund (the Stable Support Plan Program 20220810161616001), and the Strategic Priority Research Program of Chinese Academy of Sciences (XDB30000000). the Fundamental Research Funds for the

Central Universities, and the Research Funds of Renmin University of China [Grant No. 22XNKJ30 (W.J.)]. Calculations were performed at the Physics Lab of High-Performance Computing of Renmin University of China and the Beijing Supercomputer Center. We also acknowledge HZWTECH for providing computation facilities.

REFERENCES

- 1 Kennes, D. M. *et al.* Moiré heterostructures as a condensed-matter quantum simulator. *Nature Physics* **17**, 155-163 (2021).
- 2 Naik, M. H. & Jain, M. Ultraflatbands and shear solitons in moiré patterns of twisted bilayer transition metal dichalcogenides. *Physical review letters* **121**, 266401 (2018).
- 3 Wu, F., Lovorn, T., Tutuc, E. & MacDonald, A. H. Hubbard model physics in transition metal dichalcogenide moiré bands. *Physical review letters* **121**, 026402 (2018).
- 4 Zhang, Z. *et al.* Flat bands in twisted bilayer transition metal dichalcogenides. *Nature Physics* **16**, 1093-1096 (2020).
- 5 Wang, L. *et al.* Correlated electronic phases in twisted bilayer transition metal dichalcogenides. *Nature materials* **19**, 861-866 (2020).
- 6 Li, H. *et al.* Imaging two-dimensional generalized Wigner crystals. *Nature* **597**, 650-654 (2021).
- 7 Seyler, K. L. *et al.* Signatures of moiré-trapped valley excitons in MoSe₂/WSe₂ heterobilayers. *Nature* **567**, 66-70 (2019).
- 8 Jin, C. *et al.* Observation of moiré excitons in WSe₂/WS₂ heterostructure superlattices. *Nature* **567**, 76-80 (2019).
- 9 Marcellina, E. *et al.* Evidence for moiré trions in twisted MoSe₂ homobilayers. *Nano Letters* **21**, 4461-4468 (2021).
- 10 Bistritzer, R. & MacDonald, A. H. Moire bands in twisted double-layer graphene. *Proc Natl Acad Sci U S A* **108**, 12233-12237 (2011). <https://doi.org/10.1073/pnas.1108174108>
- 11 Cao, Y. *et al.* Nematicity and competing orders in superconducting magic-angle graphene. *science* **372**, 264-271 (2021).
- 12 Kapfer, M. *et al.* SI:Programming twist angle and strain profiles in 2D materials. *Science* **381**, 677-681 (2023). <https://doi.org/10.1126/science.ade9995>
- 13 Uri, A. *et al.* Mapping the twist-angle disorder and Landau levels in magic-angle graphene. *Nature* **581**, 47-52 (2020).
- 14 Grover, S. *et al.* Chern mosaic and Berry-curvature magnetism in magic-angle graphene. *Nature physics* **18**, 885-892 (2022).
- 15 Turkel, S. *et al.* Orderly disorder in magic-angle twisted trilayer graphene. *Science* **376**, 193-199 (2022).
- 16 Pantaleón, P. A., Low, T. & Guinea, F. Tunable large Berry dipole in strained twisted bilayer graphene. *Physical Review B* **103**, 205403 (2021).
- 17 de Jong, T. A. *et al.* Imaging moiré deformation and dynamics in twisted bilayer graphene. *Nature Communications* **13**, 70 (2022).
- 18 Nakatsuji, N. & Koshino, M. Moiré disorder effect in twisted bilayer graphene. *Physical Review B* **105**, 245408 (2022).
- 19 Kwan, Y. H. *et al.* Kekulé spiral order at all nonzero integer fillings in twisted bilayer graphene. *Physical Review X* **11**, 041063 (2021).
- 20 Lau, C. N., Bockrath, M. W., Mak, K. F. & Zhang, F. Reproducibility in the fabrication and physics of moiré materials. *Nature* **602**, 41-50 (2022).
- 21 Gao, Q., Dong, J., Ledwith, P., Parker, D. & Khalaf, E. Untwisting moiré physics: Almost ideal bands and fractional Chern insulators in periodically strained monolayer graphene. *Physical Review Letters* **131**, 096401 (2023).

- 22 Li, Y. *et al.* One-Dimensional Electronic Flat Bands in Untwisted Moiré Superlattices. *Advanced Materials*, 2300572 (2023).
- 23 Tao, Z.-R. *et al.* Untwisted restacking of two-dimensional metal-organic framework nanosheets for highly selective isomer separations. *Nature Communications* **10**, 2911 (2019).
- 24 Lee, C., Wei, X., Kysar, J. W. & Hone, J. Measurement of the elastic properties and intrinsic strength of monolayer graphene. *science* **321**, 385-388 (2008).
- 25 Wei, Y. & Yang, R. Nanomechanics of graphene. *National Science Review* **6**, 324-348 (2019).
- 26 Cadelano, E., Palla, P. L., Giordano, S. & Colombo, L. Nonlinear elasticity of monolayer graphene. *Physical review letters* **102**, 235502 (2009).
- 27 Wei, X., Fragneaud, B., Marianetti, C. A. & Kysar, J. W. Nonlinear elastic behavior of graphene: Ab initio calculations to continuum description. *Physical Review B* **80**, 205407 (2009).
- 28 Khestanova, E., Guinea, F., Fumagalli, L., Geim, A. & Grigorieva, I. Universal shape and pressure inside bubbles appearing in van der Waals heterostructures. *Nature communications* **7**, 12587 (2016).
- 29 Tyurnina, A. V. *et al.* Strained bubbles in van der Waals heterostructures as local emitters of photoluminescence with adjustable wavelength. *ACS photonics* **6**, 516-524 (2019).
- 30 Zabel, J. *et al.* Raman spectroscopy of graphene and bilayer under biaxial strain: bubbles and balloons. *Nano letters* **12**, 617-621 (2012).
- 31 Huang, Y. *et al.* Universal mechanical exfoliation of large-area 2D crystals. *Nature communications* **11**, 2453 (2020).
- 32 Lloyd, D. *et al.* Band gap engineering with ultralarge biaxial strains in suspended monolayer MoS₂. *Nano letters* **16**, 5836-5841 (2016).
- 33 Kerelsky, A. *et al.* Maximized electron interactions at the magic angle in twisted bilayer graphene. *Nature* **572**, 95-100 (2019).
- 34 Po, H. C., Zou, L., Vishwanath, A. & Senthil, T. Origin of Mott insulating behavior and superconductivity in twisted bilayer graphene. *Physical Review X* **8**, 031089 (2018).
- 35 Koshino, M. *et al.* Maximally localized wannier orbitals and the extended hubbard model for twisted bilayer graphene. *Physical Review X* **8**, 031087 (2018).
- 36 Trambly de Laissardière, G., Mayou, D. & Magaud, L. Localization of Dirac electrons in rotated graphene bilayers. *Nano letters* **10**, 804-808 (2010).
- 37 Nam, N. N. & Koshino, M. Lattice relaxation and energy band modulation in twisted bilayer graphene. *Physical Review B* **96**, 075311 (2017).
- 38 Zhou, Y. C., Zhang, H. L. & Deng, W. Q. A 3N rule for the electronic properties of doped graphene. *Nanotechnology* **24**, 225705 (2013). <https://doi.org/10.1088/0957-4484/24/22/225705>
- 39 Michaud-Rioux, V., Zhang, L. & Guo, H. RESCU: A real space electronic structure method. *Journal of Computational Physics* **307**, 593-613 (2016).
- 40 Plimpton, S. Fast parallel algorithms for short-range molecular dynamics. *Journal of computational physics* **117**, 1-19 (1995).
- 41 Tersoff, J. Modeling solid-state chemistry: Interatomic potentials for multicomponent systems. *Physical review B* **39**, 5566 (1989).

- 42 Kolmogorov, A. N. & Crespi, V. H. Registry-dependent interlayer potential for graphitic systems. *Physical Review B* **71**, 235415 (2005).
- 43 Jussila, H., Yang, H., Granqvist, N. & Sun, Z. Surface plasmon resonance for characterization of large-area atomic-layer graphene film. *Optica* **3** (2016). <https://doi.org:10.1364/optica.3.000151>
- 44 Lei, L. *et al.* Electronic Janus lattice and kagome-like bands in coloring-triangular MoTe₂ monolayers. *Nature Communications* **14**, 6320 (2023).
- 45 Zhang, S. *et al.* Kagome bands disguised in a coloring-triangle lattice. *Physical Review B* **99**, 100404 (2019).